Supporting Information for High-Resolution Numerical Modelling of Barotropic Global Ocean Tides for Satellite Gravimetry

R. Sulzbach[1,2], H. Dobslaw[1], M. Thomas[1,2]

[1]Deutsches Geoforschungszentrum (GFZ), Telegrafenberg, 14473 Potsdam

[2]Institut für Meteorologie, Freie Universität Berlin (FUB), Carl-Heinrich-Becker-Weg 6-10, 12165 Berlin

Contents of this file

Introduction In this study wavedrag dissipation is mediated in terms of a tensor derived by (Nycander, 2005). We briefly summarize its creation in Sect. SI1. The creation of the bathymetric dataset from high-resolution RTOPO2-data (Schaffer et al., 2016) is motivated and explained in Sect. SI2, before the tidal potential cataloge employed for the tidal simulations in this study is discussed and presented in Sect. SI3.

Methods SI1. Nycander-Wavedrag

The dissipation tensor is defined by

$$\mathbb{C} = \frac{N_B}{4\pi}\sqrt{1-\frac{f^2}{\omega^2}}\begin{pmatrix} 2\left(\partial x_1 H\ \partial x_1 j\right) & \partial x_1 H\ \partial x_2 j + \partial x_2 H\ \partial x_1 j \\ \partial x_1 H\ \partial x_2 j + \partial x_2 H\ \partial x_1 j & 2\left(\partial x_2 H\ \partial x_2 j\right) \end{pmatrix} \tag{1}$$

Here N_B is buoyancy frequency evaluated at the sea floor and x_i are local orthogonal coordinates that we will identify with east and north directions. Please note that the direct dependence on ω renders $\mathbb{C}$ non-local in time. The function

$$\boldsymbol{\nabla} j(\mathbf{x}) = \int dA' g_a(|\mathbf{x}-\mathbf{x}'|)\boldsymbol{\nabla} H(\mathbf{x}') \tag{2}$$

is calculated by a convolution integral with a non-homogeneous Green's function $g_a(r) = \frac{1}{a}G(\frac{r}{a})$. Within the Green's function $G(x)$ is defined as

$$G(x) = \frac{1}{x} - \frac{\sqrt{\pi}}{2}e^{-x^2/8}I_0(\frac{x^2}{8}), \tag{3}$$

where I_0, the modified Bessel function of first kind, serves as a wave filter. The explicit space dependence of g_a originates from the length scale $a(\phi,\lambda) = \beta\overline{N}H/(\pi\sqrt{\omega^2-f^2})$, that contains information about bathymetry $H(\mathbf{x})$, depth averaged buoyancy frequency $\overline{N}(\phi,\lambda)$ as well as the tidal frequency ω. We decided not to collapse the wave drag-parametrization to a scalar form, which has been shown to slightly improve the model's accuracy (Buijsman et al., 2015) in order to avoid including any results derived from altimetric data (in this case data-constrained ocean currents) to keep the model in a form that can be also flexibly applied to paleo settings. The calculation of $\mathbb{C}$ is carried out following the improved numerical scheme described in Green and Nycander (2013) at a resolution of $1/30°$ and then interpolated conservatively to the coarser $1/12°$ $(1/6°, 1/3°)$-resolution used for tidal modeling. The convolution integral (3) is therby truncated at $r = 5a$.

Methods SI2. Global Bathymetry Interpolation

Highly resolved bathymetric data (Schaffer et al., 2016) is regridded to the tidal model's lower resolution ($\frac{1}{12}$...1°). Seeking an algorithm that optimally conserves the bathymetric information obtained at high resolution, we consider the shallow-water equations in the abbreviated form

$$\left(\left(\hat{\mathcal{O}}_1 + \hat{\mathcal{O}}_2(H)\right)\ \boldsymbol{\zeta}^{\omega} - \mathbf{F}_0\right) e^{i\omega t} = 0 \tag{4}$$

where three groups of operators are defined: Group $\hat{\mathcal{O}}_2(H)$, that explicitly depends on the bathymetric function H , group $\hat{\mathcal{O}}_1$ not depending on H and the external forcing $\mathbf{F}_0 = -g\nabla\zeta_{eq}$, additionally independent off $\boldsymbol{\zeta}$. We further assume $H = H_0 + \delta B$ and $\boldsymbol{\zeta}^{\omega} = \boldsymbol{\zeta}_0 + \delta\boldsymbol{\zeta}$, thus introducing a tiny bathymetric disturbance δB to a known bathymetric function H_0, that causes an exiguous disturbance $\delta\boldsymbol{\zeta}$ in the corresponding solution vector $\boldsymbol{\zeta}_0$. Since this disturbance is small, $\delta\boldsymbol{\zeta}$ is determined by

$$\left(\mathcal{O}_1 + \mathcal{O}_2(H_0 + \delta B)\right)\delta\boldsymbol{\zeta} = \begin{pmatrix} r|v_0|\frac{1}{H_0^2}\mathbf{v}_0 \\ \mathbf{v}_0 \cdot \boldsymbol{\nabla} + \frac{(\boldsymbol{\nabla}H_0)\mathbf{v}_0 - \partial_t\zeta_0}{H_0} \end{pmatrix} \delta B \equiv \mathbf{F}_{\epsilon}(\delta B, H_0, \boldsymbol{\zeta}_0). \tag{5}$$

This equation describes shallow water dynamics for $\delta\boldsymbol{\zeta}$ driven by the external force $\mathbf{F}_{\epsilon}$. We define the bathymetric disturbance introduced by a drastical reduction of initial resolution as

$$\delta B_{ij} = H_{ij}^{(h)} - H_{kl}^{(l)}. \tag{6}$$

Here we added the indices h/l to indicate whether the bathymetries are defined at high or low resolution. We allow both fields to be evaluated at high resolution indicated by the indices (i,j) (coarsely resolved fields are evaluated in terms of nearest-neighbor interpolation $H_{ij}^{(l)} = H_{kl}^{(l)}$ in the vicinity of $H_{kl}^{(l)}$, denoted roi(k,l)). Due to the huge resolution difference, the disturbance δB_{ij} will have a "bumpy structure" with minor differences between grid cells in one roi(k,l) and bigger jumps, where the next-neighbor

interpolation value of $H_{ij}^{(l)}$ changes.

The overall goal is to choose $H_{kl}^{(l)}$ in such way, that it minimizes the amount of tidal dynamics evoked by $\mathbf{F}_\epsilon$. Since the forcing is proportional to δB_{ij} it has a noisy structure that can be reduced best by minimizing $||\mathbf{F}_\epsilon||$ under variation of $H_{kl}^{(l)}$. The forcing operator can thus be rewritten as

$$\mathbf{F}_\epsilon^{ij} = \mathbf{F}_{res}^{ij} + \begin{pmatrix} c_1^{(kl)} \left(H_{ij}^{(h)}\right)^{-2} \\ c_2^{(kl)} \left(H_{ij}^{(h)}\right)^{-1} \end{pmatrix} \delta B_{ij}, \text{with } (i,j) \in \text{roi}(k,l) \tag{7}$$

where the complex $c_1^{(kl)}, c_2^{(kl)}$ are constants depending on the local value of $\boldsymbol{\zeta_0}$ and $\boldsymbol{\nabla} H_0$. In the following we assume that tidal solutions are well resolved within one roi thus allowing us to treat $c_{1,2}^{(kl)}$ as constants within one roi. $\mathbf{F}_{res}^{ij}$ contains all forces that do not depend on the absolute depth value $H_{ij}^{(h)}$.

Eq. (7) states that the individual contributions to the noisy forcing will be proportional to δB_{ij} but weighted with individual weights that are proportional to H_0^{-1} and H_0^{-2} multiplied with coefficients $c_{1,2}$, respectively. We concentrate on the contribution proportional to H_0^{-1} as it orginates from the conservation of mass as a fundamental principle of hydrodynamics. We only have to evaluate the third vector component in terms of the $||\ ||^2$-norm, yielding

$$\partial_{H_{kl}^{(l)}} || \left(\mathbf{F}_\epsilon - \mathbf{F}_{res}\right) \cdot \mathbf{e}_3 || = \partial_{H_{kl}^{(l)}} \sum_{ij} |c_2^{(kl)}|^2 \left(1 - \frac{H_{kl}^{(l)}}{H_{ij}^{(h)}}\right)^2 = 0, \tag{8}$$

resulting in the minimization condition

$$H_{kl}^{(l)} = \sum_{ij} \left(H_{ij}^{(h)}\right)^{-1} / \sum_{ij} \left(H_{ij}^{(h)}\right)^{-2}. \tag{9}$$

Eq. (9) states that individual weights inversely-proportional to the bathymetric depths are the right choice to minimize resolution dependent disturbances. Please not that a consideration of terms proportional to c_1 instead of c_2 would lead to a similar result with

powers of H_0 changed by -1, which would further increase the weight of shallow water grid cells. In the light of this finding we want to stress that Eq. 7 basically proposes to perform a resolution reduction operation with weights that grow for shallow depths. This pronounces the well-known importance of preserving stream barriers and ridges.

The prerequisite $c_{1,2} = const.$ within one roi is only broken in coastal regions (roi's containing ocean and land), where tidal elevation can change drastically. As a byproduct of the depth-inverse regridding these roi's are directly evaluated as dry (shrinking ocean area) leading to the problem of closing narrow passages as, e.g., the Straight of Gibraltar. We outrun this problem by using weights proportional to depth in coastal areas (first-order conservative interpolation). This scheme evaluates roi's containing at least one wet grid cell as wet (growing ocean area) and conserves the cross-section of straights. We finally remark that differences between the discussed scheme and first-order conservative remapping (compare Fig. S1) are small at a resolution of $\frac{1}{12}^\circ$ but become much more significant at lower resolution.

Despite the partially rough approximations and assumptions, these considerations resulted in a physically meaningful and versatile interpolation technique, so that bathymetric maps for any given spatial grid with rotated poles can be evaluated in an automatic way.

Methods SI3. Selected Partial Tides Available from HW95

The HW95 (Hartmann & Wenzel, 1995) Tide-Generating Potential was implemented in TiME. We decided to shrink this catalogue to one containing all excitations with amp $> 0.005\frac{m^2}{s^2}$, (0.4 % M_2-amplitude) listed in Tabs. S1 to S4. This catalogue contains the principal 8 diurnal and semi-diurnal partial tides as well as several weaker excitations

(minor tides). The contributions of these minor tides are small, but can significantly influence sea-surface heights on the level of modern gravimetric and altimetric precision. Minor tides are often estimated by employing assumptions about the admittance functions Z_{2m} (Gérard & Luzum, 2010; Ray, 2017). We also emphasize some minor tides with particular characteristics, that might be of special interest for direct simulation.

Tides influenced by radiational excitation: Some tidal excitations experience a considerable forcing related to atmospheric processes, that are induced by solar radiation (e.g. S2). Accurate simulation of these excitations must consider additional forcing by atmospheric tides in terms of both surface pressure and wind stress.

The ψ_1-tide: This minor diurnal excitation is known as 'the problematic tide', a term introduced by R. Ray. The PSI1 ocean tide response is hard to determine due to (1) NDFW-resonance disturbed LLNs, (2) large radiational/atmospheric excitation, (3) overlap with the RP1 compound tide and (4) overlap with climate induced variation of K_1.

Tides derived by admittance extrapolation: Minor tides situated at the edges of tidal bands(e.g. $\eta_2/\epsilon_2/2Q_1/OO_1$) are usually estimated by extrapolation of the admittance function. This brings the risk of unquantified additional uncertainty by less well constrained admittance assumptions. In this paper, we showed that for the diurnal tidal band the utilization of a unconstrained model can be benecficial.

Tides originating from third degree TGP: These excitations, nominally 3MO0, M1, 3MK_2, 3MO2 and M3, represent elements of the admittance functions Z_{31}, Z_{32} and Z_{33} and cannot be derived by admittance methods from the $l = 2$- potential. Previous studies suggest enhanced resonance for several of these excitations (Ray, 2001; Cartwright,

1976), while most recently the first global maps of empirically estimated degree-3 tides illuminated their exotic admittance patterns (Ray, 2020).

References

Buijsman, M. C., Arbic, B. K., Green, J. A., Helber, R. W., Richman, J. G., Shriver, J. F., ... Wallcraft, A. (2015). Optimizing internal wave drag in a forward barotropic model with semidiurnal tides. *Ocean Model.*, *85*, 42–55. Retrieved from `http://dx.doi.org/10.1016/j.ocemod.2014.11.003` doi: 10.1016/j.ocemod.2014.11.003

Cartwright, D. E. (1976). Anomalous M1 tide at Lagos. *Nature*, *263*, 217–218.

Gérard, P., & Luzum, B. (2010). IERS Conventions (2010). *Bur. Int. Des Poids Mes. Sevres (France), Tech. Note No. 36*. Retrieved from `url:http://portal.tugraz.at/portal/page/portal/Files/i5210/files/projekte/COTAGA/TN{\_}EOT11a.pdf`

Green, J., & Nycander, J. (2013). A Comparison of Tidal Conversion Parameterizations for Tidal Models. *J. Phys. Oceanogr.*, *43*(1), 104–119. doi: 10.1175/jpo-d-12-023.1

Hartmann, T., & Wenzel, H.-G. (1995). The HW95 tidal potential catalogue. *Geophyical Res. Lett.*, *22*(24), 3553–3556.

Nycander, J. (2005). Generation of internal waves in the deep ocean by tides. *J. Geophys. Res. C Ocean.*, *110*(10), 1–9. doi: 10.1029/2004JC002487

Ray, R. D. (2001). Resonant third-degree diurnal tides in the Seas off Western Europe. *J. Phys. Oceanogr.*, *31*(12), 3581–3586. doi: 10.1175/1520-0485(2001)031⟨3581:RTDDTI⟩2.0.CO;2

Ray, R. D. (2017). On Tidal Inference in the Diurnal Band. *J. Atmos. Ocean. Technol.*, *34*(2), 437–446. doi: 10.1175/jtech-d-16-0142.1

Ray, R. D. (2020). First global observations of third-degree ocean tides. *Sci. Adv.*, *6*(48), 1–8. doi: 10.1126/sciadv.abd4744

Schaffer, J., Timmermann, R., Erik Arndt, J., Savstrup Kristensen, S., Mayer, C., Morlighem, M., & Steinhage, D. (2016). A global, high-resolution data set of ice sheet topography, cavity geometry, and ocean bathymetry. *Earth Syst. Sci. Data*, *8*(2), 543–557. doi: 10.5194/essd-8-543-2016

Table S1. HW95-excerpt Part 1

i	Doodson	f $[\frac{\circ}{h}]$	l	amp $[\frac{mm^2}{s^2}]$	name
1	055.565	0.00221	2	7.719645e+04	M0+
2	056.554	0.04107	2	1.360322e+04	Sa
3	057.555	0.08214	2	8.565377e+04	**Ssa**
4	058.554	0.12320	2	5.006949e+03	Sta
5	063.655	0.47152	2	1.859612e+04	Msm
6	065.445	0.54217	2	6.383833e+03	Mm-
7	065.455	0.54437	2	9.725014e+04	**Mm**
8	065.465	0.54658	2	6.311086e+03	Mm+
9	065.555	0.54902	3	1.042363e+04	3MO0
10	065.655	0.55366	2	5.204394e+03	NO
11	073.555	1.01590	2	1.613284e+04	Msf
12	075.355	1.08875	2	7.970438e+03	2Mm
13	075.555	1.09803	2	1.841040e+05	**Mf**
14	075.565	1.10024	2	7.633235e+04	Mf+
15	075.575	1.10245	2	7.138909e+03	Mf++
16	083.655	1.56955	2	6.693729e+03	Mstm
17	085.455	1.64241	2	3.525008e+04	Mtm
18	085.465	1.64461	2	1.460963e+04	Mtm+
19	093.555	2.11393	2	5.630068e+03	MSqm

Table S2. HW95-excerpt Part 2

i	Doodson	f $[\frac{\circ}{h}]$	l	amp $[\frac{mm^2}{s^2}]$	name
20	125.755	12.85429	2	1.298572e+04	2Q1
21	127.555	12.92714	2	1.565932e+04	SGM1
22	135.645	13.39645	2	1.850638e+04	Q1-
23	135.655	13.39866	2	9.813054e+04	**Q1**
24	137.455	13.47151	2	1.862609e+04	RO1
25	145.545	13.94083	2	9.668862e+04	O1-
26	145.555	13.94304	2	5.125255e+05	**O1**
27	147.555	14.02517	2	6.680540e+03	TAU1
28	155.455	14.48741	2	1.448964e+04	LK1
29	155.555	14.49205	3	7.832888e+03	M1
30	155.655	14.49669	2	4.028717e+04	NO1
31	155.665	14.49890	2	8.085297e+03	NO1+
32	157.455	14.56955	2	7.709119e+03	CHI1
33	162.556	14.91786	2	1.393773e+04	PI1
34	163.555	14.95893	2	2.384377e+05	**P1**
35	164.556	15.00000	2	5.636309e+03	S1
36	165.545	15.03886	2	1.426815e+04	K1-
37	165.555	15.04107	2	7.205113e+05	**K1**
38	165.565	15.04328	2	9.778461e+04	K1+
39	166.554	15.08214	2	5.638973e+03	PSI1
40	167.555	15.12321	2	1.025988e+04	PHI1

Table S3. HW95-excerpt Part 3

i	Doodson	f $[\frac{\circ}{h}]$	l	amp $[\frac{mm^2}{s^2}]$	name
41	173.655	15.51259	2	7.706830e+03	TET1
42	175.455	15.58544	2	4.030173e+04	J1
43	175.465	15.58765	2	7.988353e+03	J1+
44	183.555	16.05696	2	6.683724e+03	SO1
45	185.555	16.13910	2	2.204454e+04	OO1
46	185.565	16.14131	2	1.412517e+04	OO1+
47	227.655	27.42383	2	9.129880e+03	EPS2
48	235.755	27.89535	2	3.130700e+04	2N2
49	237.555	27.96821	2	3.778507e+04	MUE2
50	245.555	28.43509	3	7.604162e+03	3MK2
51	245.645	28.4375	2	8.832390e+03	N2-
52	245.655	28.43973	2	2.365822e+05	**N2**
53	247.455	28.51258	2	4.494047e+04	NUE2
54	255.545	28.98190	2	4.610383e+04	M2-
55	255.555	28.98410	2	1.235635e+06	**M2**
56	263.655	29.45563	2	9.111517e+03	LAM2
57	265.455	29.52848	2	3.492889e+04	L2
58	265.555	29.53312	3	7.013920e+03	3MO2
59	265.655	29.53776	2	8.730910e+03	KNO2
60	272.556	29.95893	2	3.360070e+04	T2
61	273.555	30.00000	2	5.748299e+05	**S2**

Table S4. Selection of partial tides from HW95, that can be used with TiME, where amp $= \sqrt{(S_i^{lm})^2 + (C_i^{lm})^2}$ (where S_i^{lm}, C_i^{lm} are listed in HW95). Here, all partial tides with amplitudes bigger than $0.005 \frac{m^2}{s^2}$ are considered, with potential extension to arbitrary tides in HW95. Major tidal constituents are **highlighted**.

i	Doodson	f $[\frac{\circ}{h}]$	l	amp $[\frac{mm^2}{s^2}]$	name
62	275.555	30.08214	2	1.561924e+05	**K2**
63	275.565	30.08434	2	4.655091e+04	K2+
64	275.575	30.08655	2	5.060029e+03	K2++
65	285.455	30.62651	2	8.737090e+03	ETA2
66	355.555	43.47616	3	1.496874e+04	M3

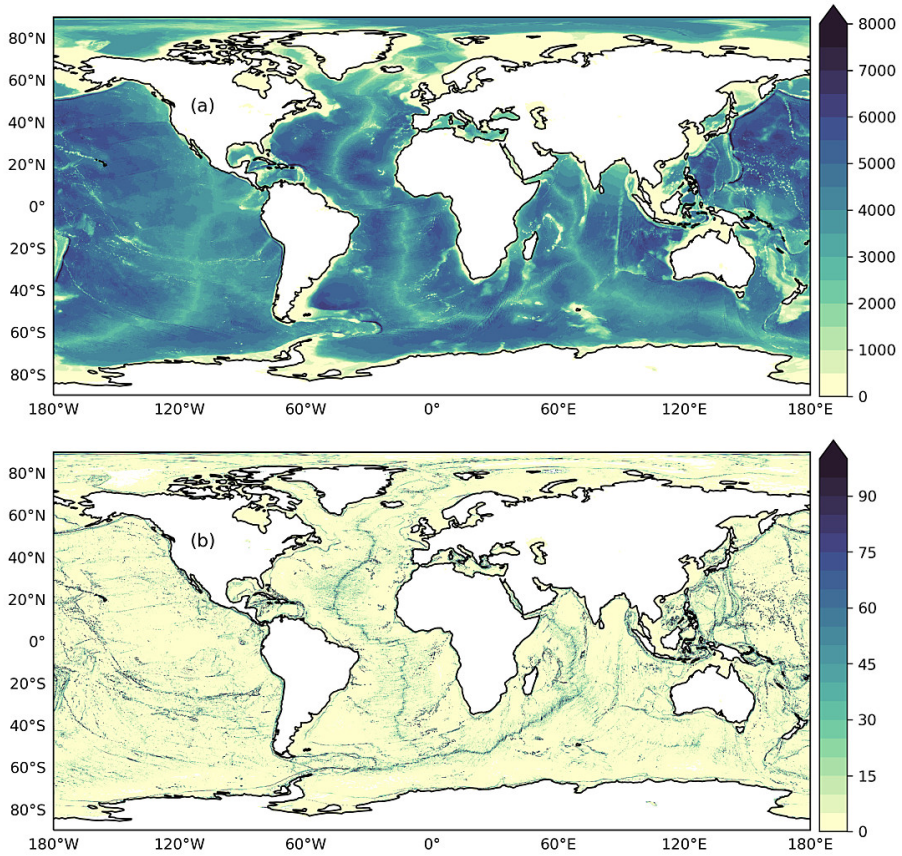

Figure S1. Utilized global Rtopo2 bathymetry including the sub-ice-shelf water column (a). Differences between bathymetry obtained by first order conservative remapping minus the dataset produced with the described method (see Sect. SI2) is shown on (b). Please note that difference are entirely positive as the described method puts increased weights on small water depths. Data was interpolated to TiME's default resolution of $\frac{1}{12}^{\circ}$. All units are in meters.